Supporting Information

High capacity, reversible alloying reactions in SnSb/C nanocomopsites for Na-ion battery applications

Lifen Xiao,[a,b] Yuliang Cao,[a,c] Jie Xiao,[a] Wei Wang,[a] Libor Kovarik,[a] Zimin Nie,[a] Jun Liu[a,*]

[a]*Pacific Northwest National Laboratory, Richland, WA 99352, USA*
[b]*College of Chemistry, Central China Normal University, Wuhan 430079, P. R. China*
[c]*College of Chemistry and Molecular Science, Wuhan University, Wuhan 430072, P. R. China*
E-mail: Jun.Liu@pnnl.gov

Experimental Section

Material preparation. Sn power (99.8% purity, <45μm, Aldrich), Sb powder (99.5% purity, -100 mesh Aldrich) and super P (TIMCAL, Graphite & Carbon Inc.) were used as received. The Sn/C, Sb/C, and SnSb/C nanocomposites and pure carbon sample were prepared by high-energy mechanical milling (HEMM, 8000 M Mixer/Mill, SPEX, USA) under an argon atmosphere for 8 h. The metal:carbon black weight ratio was set to 7:3. In the case of SnSb/C, the Sn:Sb was 1:1 by molar ratio. The Sn and Sb bulk samples were respectively prepared by mixing Sn or Sb with carbon black in a weight ratio of 7:3.

Structure Characterization. The crystalline structures of the as-prepared nanocomposites were characterized by x-ray diffraction (XRD, Philips Xpert X-ray diffractometer using Cu Kα radiation at λ=1.54 Å). The high-resolution TEM imaging was performed with a FEI Titan 80-300 microscope operated at 300 kV. The instrument is equipped with a CEOS GmbH double-hexapole aberration corrector for the probe-forming lens, which allows imaging with 0.1-nm resolution in scanning transmission electron microscopy (STEM) mode. The STEM images were acquired on high angle annular dark field (HAADF) with an inner collection angle of 52 mrad. The elemental analysis was performed using an EDAX Si (Li) EDS detector and FEI TIA analysis software.

Electrochemical measurement. The anodes were prepared by mixing 80 wt% metal/carbon composite, 10 wt% super P, and 10 wt% carboxymethyl cellulose (CMC, 0.01g mL^{-1}) to form a slurry, which then was applied to copper (Cu) foil and dried at 70 ^{o}C overnight under vacuum. The electrochemical cells were assembled in an argon-filled glove box using 2325 coin cells with Na metal as the counter electrodes, 1 M $NaClO_4$ dissolved in ethylene carbonate (EC)/dimethyl carbonate (DMC) (1:1 by volume) as the electrolyte, and Celgard 3501 microporous membrane as the separator. The galvanostatic charge-discharge test was conducted using a BT-2043 Arbin Battery Testing System. Cyclic voltammograms were obtained using a SI 1287 electrochemical interface (Solartron).

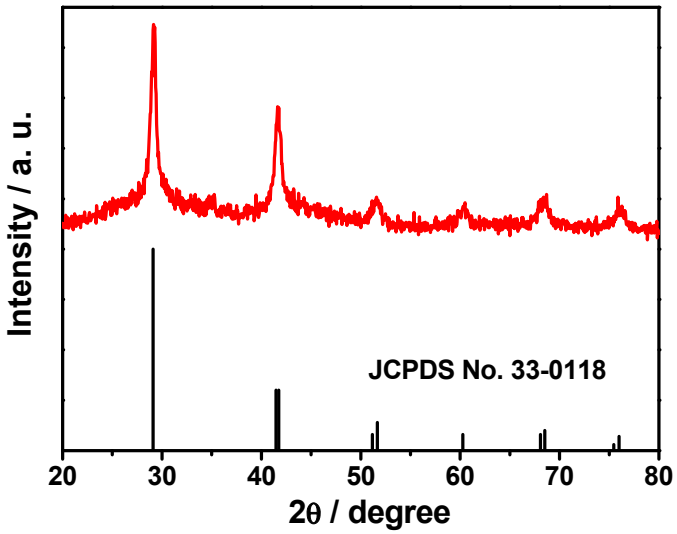

Fig. S1. XRD patterns of the SnSb/C nanocomposite synthesized by HEMM for 8 h.

Fig. S1 displays the experimental XRD patterns of the SnSb/C nanocomposites. The XRD peaks can be basically indexed by a signal phase rhombohedra SnSb (JCPDS No. 33-0118). No obvious characteristics for Sb-Fe or Sn-Fe alloy impurities are observed. No metallic Sn or Sb peaks are observed in the SnSb/C composite, indicating that Sn and Sb has formed alloy completely after the HEMM method.

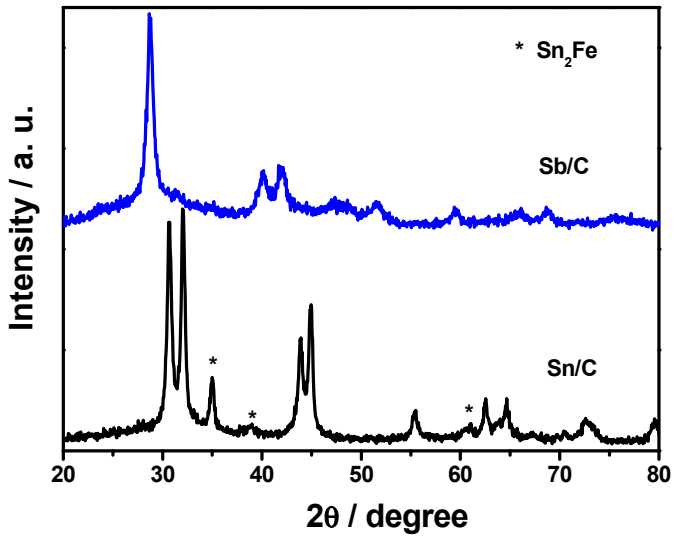

Fig. S2. XRD patterns of the Sn/C and Sb/C nanocomposites synthesized by HEMM for 8 h

Fig. S2 shows the XRD patterns of the Sn/C and Sb/C nanocomposites. For Sn/C, the main double peaks located at 30.6° and 32.0° are attributed to the tetragonal Sn (JCPDS No. 65-2631). The other set of peaks as the strongest peak occurs at 35.1° is attributed to some Sn_2Fe alloy impurity (JCPDS No. 65-0374). The Fe impurity was introduced during the mechanical milling process. For Sb/C, the XRD peaks can be basically indexed by a single-phase rhombohedra Sb (JCPDS No. 85-1324). No obvious characteristics for Sb-Fe alloy impurities are observed.

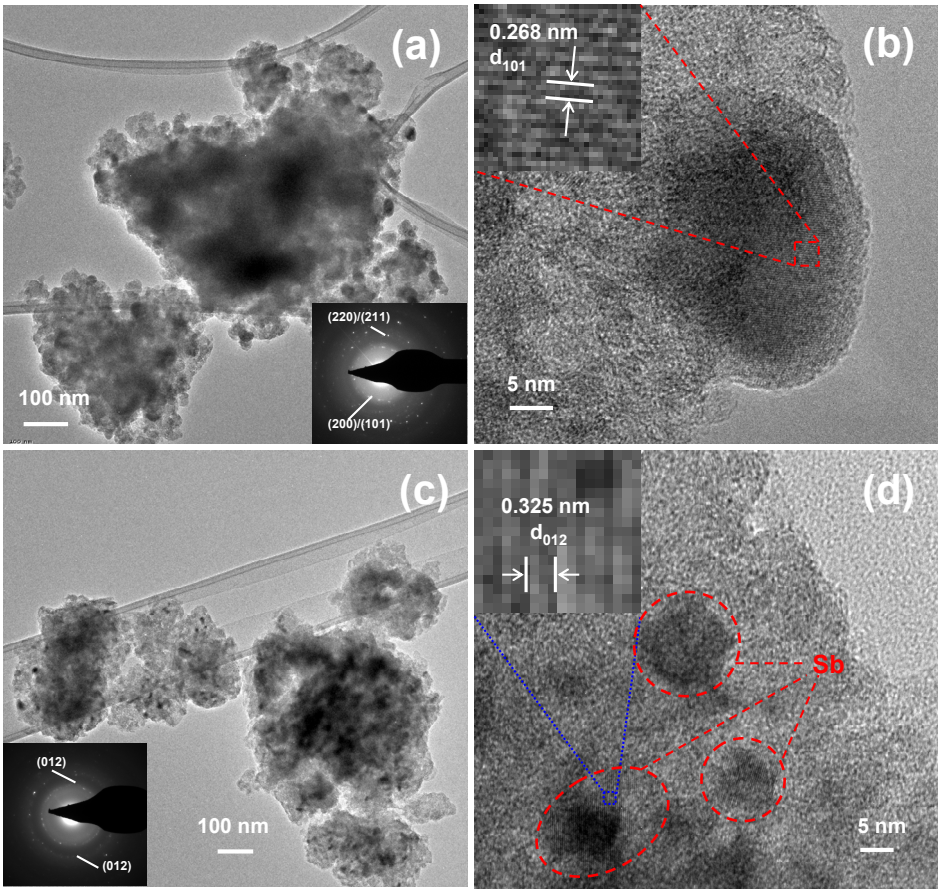

Fig. S3. TEM and HRTEM images of the nanocomposties: (a, b) Sn/C and (c, d) Sb/C

The TEM and the SAED images show that Sn/C and Sb/C (Fig. S3a, c) are formed by large agglomerates with submicron dimensions, and are composed of metal nanoparticles well dispersed in the carbon matrix. The HRTEM image shows that the metallic Sn particles in the Sn/C composite are not very uniform in diameter. Some particles are larger than 10 nm, and there are many particles smaller than 2 nm. The metallic Sb in the Sb/C composite shows a more even dimensional distribution (less than 10 nm). This may arise from the different attributions of the metallic Sn and Sb. Sb is brittle and Sn is ductile, which makes Sb easy to be pulverized while Sn is not.

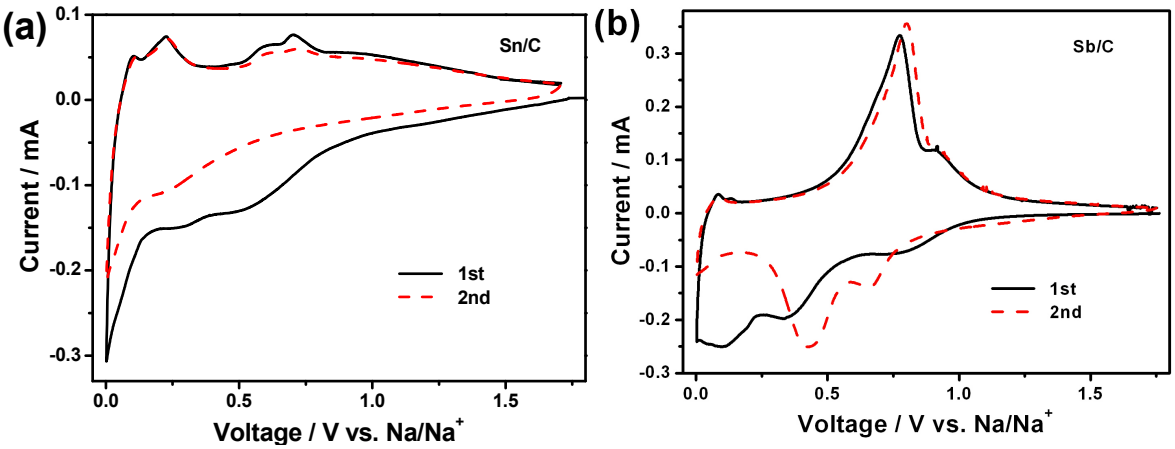

Fig. S4. Initial two cyclic voltammogram curves (CVs) of the (a) Sn/C and (b) Sb/C nanocomposite electrodes from open circuit voltage to 0.0 V vs. Na/Na^+ at a scan rate of 0.1 mV s^{-1}

Fig. S4 shows the cyclic voltammograms of the Sn/C, Sb/C nanocomposite electrodes conducted at a scan rate of 0.1 mV s^{-1} from the open circuit voltage to 0 V vs. Na/Na^+. In the case of the Sn/C nanocomposite (Fig. S4a), the first cathodic scan shows a wide irreversible current peak in the range of 0.8 to 0.4 V, which corresponds to the decomposition of electrolyte to form solid-electrolyte interface (SEI) films. Under continuous scan, two intensive reductive peaks occurred at approximately 0.28 V and 0.00 V. These peaks correspond to the reaction between Sn and Na to form Na-Sn alloy. From the reverse scan, four oxidative peaks can be clearly distinguished at 0.10, 0.22, 0.60 and 0.70 V, respectively, indicating that the phase transition during the dealloying process is more distinct. The Na-Sn alloying-dealloying processes are qualitatively analogous to the Li-Sn counterpart, together with low Na-alloying potentials. As in the Na-Sn binary alloy phase diagrams, the main stable phases are α-NaSn, Na_9Sn_4, Na_3Sn, and $Na_{15}Sn_4$. It can be inferred that the four oxidative peaks at 0.10, 0.22, 0.60 and 0.70 V are attributed to the $Na_{15}Sn_4$, Na_3Sn Na_9Sn_4, and α-NaSn dealloying reactions, respectively. The reductive peak positioned at 0.28 V corresponds to the merging alloy phases of Na_9Sn_4 and α-NaSn, and the reductive peak close to 0.00 V is assigned to the merging alloy phases of $Na_{15}Sn_4$ and Na_3Sn, so Sn can alloy with Na to uptake 3.75 Na per Sn atom in accordance with the reaction of $Sn + 3.75Na^+ + 3.75e^- \rightarrow Na_{3.75}Sn$ ($Na_{15}Sn_4$), thus leading to a total theoretical Na storage capacity of 847 mAh g^{-1}.

The first negative scan of the Sb/C nanocomposite shown in Fig. S4b also shows an irreversible reductive peak located at approximately 0.8 V, which as discussed above corresponds to the decomposition of electrolyte to form SEI films. Two another reductive peaks are observed at 0.34 and 0.12 V, while the relevant oxidative peaks occurring at 0.77 and 0.90 V, respectively, manifest two pairs of reversible Na-Sb alloying and dealloying reactions. During the second scan, the two reductive peaks shift to 0.66 V and 0.43 V, respectively. This shift reveals that the onward alloying process displays significantly reduced polarization, indicating a possible rearrangement of the electrode structure occurring in the first reaction, which improves the electrode kinetics of

the successive reaction. Compared with the Na-Sb phase diagram, the two pairs of redox peaks can be attributed to the two stable alloy phases of NaSb (0.43 V, 0.77 V) and Na_3Sb (0.66 V, 0.90 V), respectively, which can store up a maximum three Na atoms in per Sb atom in accordance with the reaction of $Sb + 3Na^+ + 3e^- \rightarrow Na_3Sb$. This yields a total specific capacity of 660 mAh g^{-1}. Although the CV shape is very similar to that of Li-Sb, the actual alloying-dealloying process of Na-Sb adopts a sequence of Sb to NaSb to Na_3Sb or *vice versa*, rather than from Sb to Li_2Sb to Li_3Sb or *vice versa*.

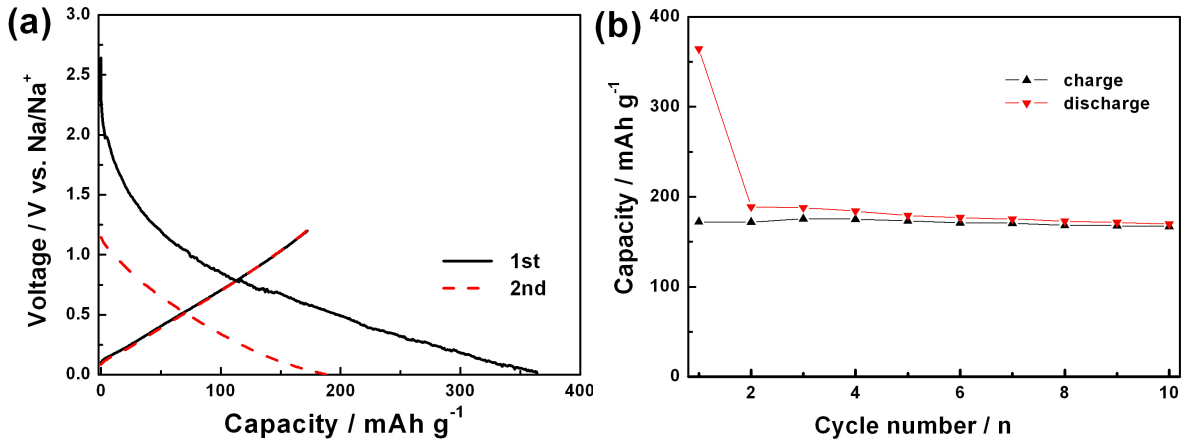

Fig. S5. Electrochemical properties of the pure carbon black (super P) obtained by HEMM for 8 h. (a) Initial two charge/discharge profiles. (b) Capacity as a function of cycles.

Fig. S5a shows the initial two discharge/charge profiles of the carbon black electrode between 0.0 and 1.2 V vs. Na/Na^+ at a current rate of 100 mA g^{-1}. The Na insertion/extraction voltage is primarily below 0.7 V. In addition, the electrode displays a very large initial irreversible capacity as the columbic efficiency is only 47%. This is common when various carbons used as Na insertion electrodes, which will great compromise their practice. Fig. S5b shows that the carbon black electrode can deliver a stable reversible capacity of 172 mAh g^{-1}.

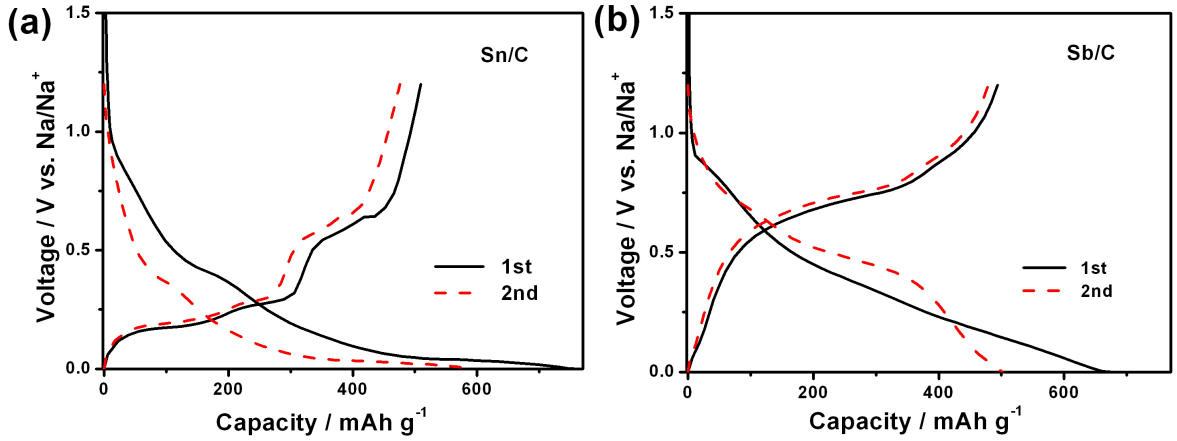

Fig. S6. The initial two discharge/charge profiles of the (a) Sn/C and (b) Sb/C nanocomposite electrodes between 0.0 and 1.2 V vs. Na/Na^+ at a current rate of 100 mA g^{-1}

Fig. S6 presents the initial two discharge/charge profiles of the Sn/C and Sb/C nanocomposite electrodes cycled between 0 and 1.2 V at a constant current density of 100 mA g^{-1}. The voltage plateaus are reflected as peaks in the CV curves. The voltage profiles of Sn/C nanocomposite shown in Fig. S6a clearly show two discharge and four charge plateaus, reflecting the stepwise Na-Sn alloy phase transition processes. The first charge recovers a reversible capacity of 509 mAh g^{-1}. After deducting the capacity associated to carbon black, Sn individually can offer a capacity of 653 mAh g^{-1}, which is about 77.1% of the theoretical capacity of 847 mAh g^{-1} based on the $Na_{15}Sn_4$. For Sb/C nanocomposite (Fig. S6b), the two discharge/charge plateaus correspond to the two couple peaks in CV curves. The initial reversible capacity is 494 mAh g^{-1}; Sb individually can offer a capacity of 631 mAh g^{-1}, which is equivalent to 95.6% of the theoretical capacity based on the Na_3Sb (660 mAh g^{-1}). Fig. S6a and b also demonstrate that the initial coulombic efficiencies are 66.6 and 72.9%, which increase to 81.2 and 95.8% at the second cycle for the Sn/C and Sb/C nanocomposites, respectively.

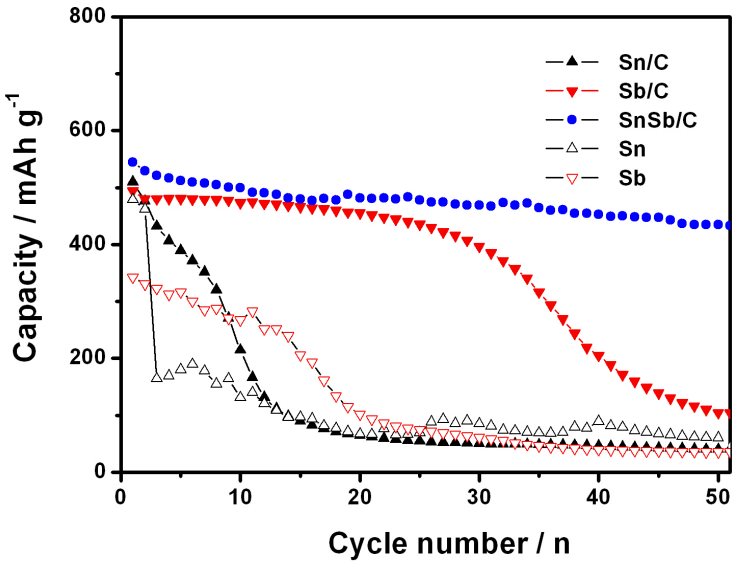

Fig. S7. Comparison of the cycling performances of the SnSb/C with the Sn/C and Sb/C nanocomposite electrodes as well as the pristine Sn and Sb electrodes between 0.0 and 1.2 V vs. Na/Na^+ at a cycling rate of 100 mA g^{-1}

Fig. S7 gives the cycling plots of the Sn/C, Sb/C, and SnSb/C naonocomposite electrodes, together with that of the pristine Sn and Sb powders for comparison. Although the bulk metallic Sn electrode can exhibit high capacity of over 460 mAh g^{-1} at the first two cycles, the capacity faded to 163 mAh g^{-1} at the third cycle. The bulk Sb electrode also shows rapid capacity decay from 342 mAh g^{-1} to less then 100 mAh g^{-1} after 20 cycles. Both bulk electrodes exhibited poor Na-recyclability. The Sn/C electrode loses 80% of its initial capacity after 13 cycles, implying that the particle downsizing improved cyclic performance only negligibly. The Sb/C electrode exhibits stable cycling up to the initial 30 cycles, as the reversible capacity attenuates from 494 to 397 mAh g^{-1}, showing 80.4% capacity retention. However, over prolonged cycling, the capacity decreased rapidly to 100 mAh g^{-1} after 50 cycles.